Journal of Advanced Marine Engineering and Technology, Vol. 50, No. 5, pp. 395~406, 2026
J. Advanced Marine Engineering and Technology (JAMET)
https://doi.org/10.5916/jamet.2026.50.5.395

ISSN 2234-7925 (Print)
ISSN 2765-4796 (Online)
Original Paper

A study on structural safety evaluation for onboard installation of a thermoelectric generator

Seung-Hun Jeong[1] · Sung-Yun Choi[2] · Myeong-Hoon Lee[3] · Yong-Sup Yun[†]

(Received August 31, 2026 ; Revised October 1, 2026 ; Accepted October 27, 2026)

Abstract: This study evaluates the structural safety of a newly developed 100 kW-class thermoelectric generator (TEG) system for onboard installation on the multi-purpose offshore demonstration vessel KOMERI1, using finite element analysis prior to installation. With the tightening and upcoming enforcement of environmental regulations by the International Maritime Organization (IMO) [1], various eco-friendly maritime technologies are being proposed, and effective reduction and recovery of the thermal energy contained in ship exhaust gas is essential. Unlike conventional waste heat recovery systems predominantly focused on steam generation, the TEG system considered in this study converts waste heat directly into electrical power. Because the developed TEG is intended to be validated through a subsequent 1,000-hour operational demonstration onboard the vessel — a validation approach expected to be more rigorous than land-based testing — its structural integrity under actual marine operating conditions must first be confirmed. This study therefore performs a structural safety assessment of the TEG installation structure within the vessel's funnel under 22 static and dynamic load combinations, identifies locally concentrated stresses exceeding the allowable limit in the initial configuration, and verifies that a subsequently proposed reinforcement brings all principal members within the allowable stress criteria. The results provide a basis for confirming the structural integrity of the installation prior to the planned onboard demonstration.

Keywords: Waste heat recovery, Thermoelectric generator, Structural safety, Computational analysis, Offshore demonstration

1. Introduction

In accordance with the International Maritime Organization (IMO)'s 2050 net-zero emissions strategy, the maritime industry is facing the significant challenge of achieving net-zero carbon emissions by 2050. To achieve this goal, various Energy-Saving Device (ESD) technologies have been proposed to improve the energy efficiency of ships and reduce greenhouse gas (GHG) emissions **[1]-[2]**. As one of the world's leading shipbuilding and maritime nations, South Korea has also been actively conducting research and development on various technologies to enhance ship energy efficiency and reduce carbon emissions **[3]-[5]**. ESD technologies can generally be categorized into three areas according to their application and operating principles: navigation, hull, and engine systems. Among these, technologies for engine systems have attracted considerable attention because of their potential to minimize energy losses from the main engine and recover otherwise wasted energy.

In particular, the exhaust gas discharged from a ship's main engine contains a considerable amount of high-temperature thermal energy. Recovering this waste heat and converting it into useful energy can improve the overall energy efficiency of the ship while reducing fuel consumption and GHG emissions. Conventional waste heat recovery technologies primarily utilize the thermal energy of exhaust gas to generate steam or a working fluid, which is subsequently used to drive a turbine. However, such systems may have limitations in terms of system complexity, installation space, and maintenance requirements when applied to marine vessels. Accordingly, thermoelectric generator (TEG)

† Corresponding Author (ORCID: http://orcid.org/0000-0003-4202-8127): Professor, Division of Mechanical Engineering, Korea Maritime & Ocean University, 727, Taejong-ro, Yeongdo-gu, Busan 49112, Korea, E-mail: ysyun@kmou.ac.kr, Tel: +82-51-410-4259

1 Researcher, Division of Substantiation Platform Technology Team, Korea Marine Equipment Research Institute, E-mail: shjeong@komeri.re.kr, Tel: +82-51-417-7095

2 Ph. D., Korea Organization for Innovative Eco-Friendly Ship Technology Development, Korea Marine Equipment Research Institute, E-mail: sy7.choi@komeri.re.kr, Tel: +82-51-400-5102

3 Chair Professor, Korea Institute of Corrosion Science & Technology, National Korea Maritime and Ocean University, E-mail: leemh@kmou.ac.kr, Tel: +82-51-410-5350

This is an Open Access article distributed under the terms of the Creative Commons Attribution Non-Commercial License (http://creativecommons.org/licenses/by-nc/3.0), which permits unrestricted non-commercial use, distribution, and reproduction in any medium, provided the original work is properly cited.

Copyright ⓒ The Korean Society of Marine Engineering

technology has attracted increasing attention as a waste heat recovery technology for marine applications because it can directly convert thermal energy into electrical energy without requiring mechanical moving components.

A thermoelectric generation system converts thermal energy directly into electrical energy through the thermoelectric effect induced by a temperature difference. The system can utilize the high-temperature waste heat continuously generated by the exhaust gas of a ship's main engine as an energy source. In addition, the absence of rotating components and working fluids enables a relatively simple system configuration and facilitates maintenance. The modular characteristics of TEG systems also provide potential advantages for integration with existing shipboard systems. Based on these characteristics, a marine thermoelectric generation system was developed in this study to generate electrical power by utilizing the high-temperature exhaust gas discharged from a ship's main engine as a heat source.

However, for the developed thermoelectric generation system to be installed and operated on an actual ship, it is necessary to ensure not only its power generation performance and thermoelectric conversion efficiency but also its structural integrity under marine operating conditions. During ship operation, the system is continuously subjected to various loads, including dynamic loads induced by ship motions caused by waves, and gravitational loads associated with the weight of the system and its components. Therefore, a structural safety assessment of the installation structure and major components of the thermoelectric generation system is essential to ensure its safe application onboard.

Structural assessments of equipment installed on ships have been reported mainly for large, safety-critical items. For independent Type C cargo and fuel tanks, the tanks, saddles and supporting structures have been evaluated by finite element analysis under the design accelerations prescribed in the IGC and IGF Codes, and the resulting stresses have been assessed by stress category **[6]-[8]**. Deck fittings such as D-rings have been assessed for their ultimate strength together with the surrounding deck structure **[9]**, and the dynamic characteristics of rotor sails have been examined with respect to the stiffness of their supporting structure **[10]**. Funnel structures have been investigated mainly for wind loads **[11]**, and the vibration of a SOx scrubber integrated into a funnel has been reported as a design case **[12]**. However, few studies have addressed a heavy and tall unit that is retrofitted inside an existing funnel and supported only through lugs and seats on the funnel wall, whose original members were designed for positioning and vibration restraint rather than for carrying load. Moreover, unlike cargo and fuel tanks, such equipment has no dedicated acceleration formula in the IGC or IGF Codes, so the ship-motion loads must be derived from the general hull structural rules.

Accordingly, this study aims to evaluate the structural suitability of the developed marine thermoelectric generation system for onboard installation. The contributions of this study are threefold: (i) the ship-motion accelerations at the TEG location are derived from the dynamic load cases of the IACS Common Structural Rules and applied as 22 load combinations to a funnel-mounted equipment support; (ii) the members overstressed in the initial support configuration are identified, and the effect of the reinforcement is quantified by comparing the maximum local stresses of each principal member before and after the reinforcement; and (iii) the stress classification of ASME Section VIII, Division 2 is applied to a non-pressure support structure, and its allowable limit is related to the yield criterion of the ship structural rules. The structural characteristics of the system are investigated, and a structural safety assessment is performed under the relevant installation and operational conditions. The results are expected to provide a basis for verifying the structural integrity of the developed system and supporting its practical application as a waste heat recovery technology for marine vessels.

2. Information on Demonstration Ship and Equipment

2.1 KOMERI1 Ship for Offshore Demonstration

The KOMERI1 Ship is a 17,000 DWT-class bulk carrier compliant with IMO regulations, capable of both domestic and international voyages. With a single bunkering, the vessel can sail more than 10,000 nautical miles, making it suitable for demonstration on long-distance routes. It is also an eco-friendly vessel equipped with a dual-

Table 1: Specification for KOMERI1

General Information	Ship	KOMERI1
	Type	17,000 DWT Bulk Carrier
	IMO No.	9985899
Principal Dimension	Length Overall	132.0 m
	Length between perpendiculars	126.0 m
	Breadth	23.0 m
	Depth	13.5 m
	Designed draft	9.5 m
Main Engine	Type	MAN 6S35ME-C9.7-GI
	SMCR	3,150 kW × 124.0 rpm
	NCR 90%	2,835 kW × 119.7 rpm

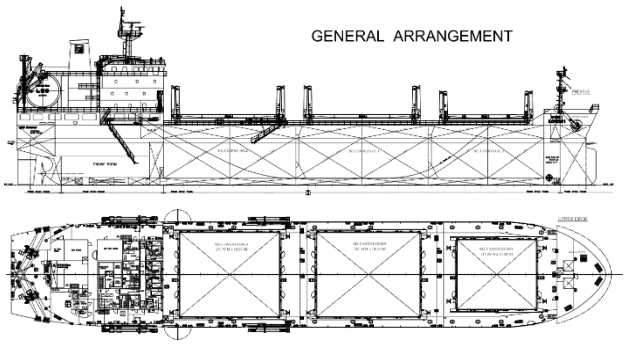

Figure 1: General Arrangement of KOMERI1

fuel engine, offering the advantage of operating on either LNG or diesel. The vessel comprises three cargo holds, which can also serve as demonstration spaces depending on the intended use. To facilitate understanding of the vessel configuration, an excerpt from the General Arrangement (GA) is presented in **Figure 1 [13]**, and the principal particulars are summarized in **Table 1 [14]**.

Operated under a bareboat charter with a shipping company, the vessel is intended to provide opportunities for obtaining track records for marine equipment that has received classification approval while engaged in commercial service.

2.2 100kW-class TEG

The thermoelectric generator (TEG) refers to a device equipped with thermoelectric modules that convert thermal energy into electrical energy. A single stage has a rated output of 20 kW, and the system was configured as five stages arranged sequentially along the exhaust gas flow, as it was developed for application to the main engine exhaust gas line of the KOMERI1 Ship. **Figure 2** illustrates the system configuration, and **Table 2** summarizes the basic specifications.

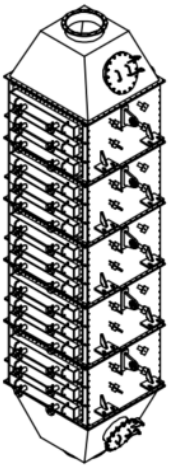

Figure 2: Schematic of 100 kW-class TEG

Table 2: Specification for TEG

Principal Dimension	Length	2,030 mm
	Breadth	2,072 mm
	Height	7,515 mm
Total Weight	Dry	Abt. 16,420 kg
	Wet	Abt. 17,250 kg

Since power is generated by the temperature difference across the thermoelectric modules, a cooling system is required. The cooling system consists of a unit that directly cools the thermoelectric modules (direct cooling) and a unit that cools the coolant (indirect cooling). These cooling systems were installed during the shipbuilding stage through design modifications. The vessel has obtained classification approval in a "Ready for TEG system" configuration, so that the developed TEG can be installed on board immediately after undergoing the inspection procedures of the Korean Register (KR).

3. Proposed Installation Plan for the TEG

The onboard installation of the TEG is planned to be carried out by mounting the unit to the funnel wall and subsequently connecting it to the previously installed TEG cooling system. The basic installation procedure is as follows, and the reference drawings corresponding to each step are presented in **Figure 3** to facilitate understanding.

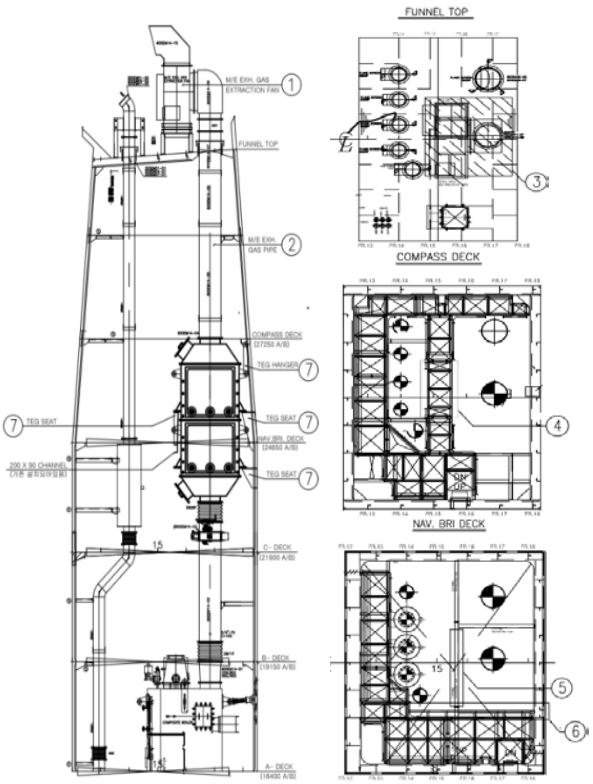

Figure 3: Schematic of TEG Installation

① Removal of the M/E exhaust gas extraction fan
② Removal of the exhaust pipe and supports above the TEG
③ Opening of the funnel top deck
④ Removal of the compass deck grating and handrails
⑤ Removal of the navigation bridge deck channel
⑥ Removal of the navigation bridge deck handrails
⑦ Fabrication and installation of the TEG seat and hanger (carlings shall be installed at the required locations after the seat is fitted to the funnel front bulkhead)
⑧ Restoration to the original condition in reverse order after installation

As indicated in ⑦, a supporting structure that connects and supports the TEG must be installed on the funnel wall, which is a factor to be taken into account during onboard installation.

4. Structural Safety Assessment for the Onboard Installation of a TEG

4.1 Geometry Model of Funnel

The TEG is applied to the downstream process of the composite boiler. The structural components available for use within the funnel are the I-shaped channel on the navigation bridge deck and the funnel wall on the bow side. Supports were constructed on the bow-side funnel wall and connected to the bow-side lugs to bear the overall load of the TEG, while a separate walkway support was designed on the stern side to handle the load and suppress vibrations.

The TEG is equipped with four pairs of lugs on the bow side and two pairs on the stern side. To facilitate a clear understanding of the lug locations, they are numbered sequentially starting with No. 1 at the bottom, as illustrated in **Figure 4**. For the TEG installation, the No. 1 lugs on the stern side were supported by installing brackets on the walkway support, whereas the No. 2 and No. 4 lugs on the bow side were supported by installing brackets on the bow-side wall structure. A total of three sets of lugs are connected to the vessel to bear the load, and for convenience, these are classified as TEG seats 1, 2, and 3.

The funnel was modeled based on the deckhouse construction drawings, incorporating the seat information. The geometric details of the TEG were provided by Kangrim Heavy Industries, the manufacturer of the system, and the connection between the TEG and the funnel was applied as shown in **Figure 5**.

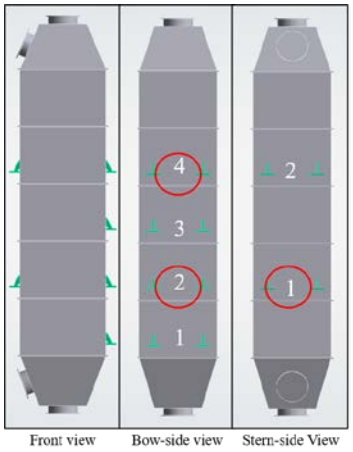

Figure 4: Lug Positions for TEG Load Support

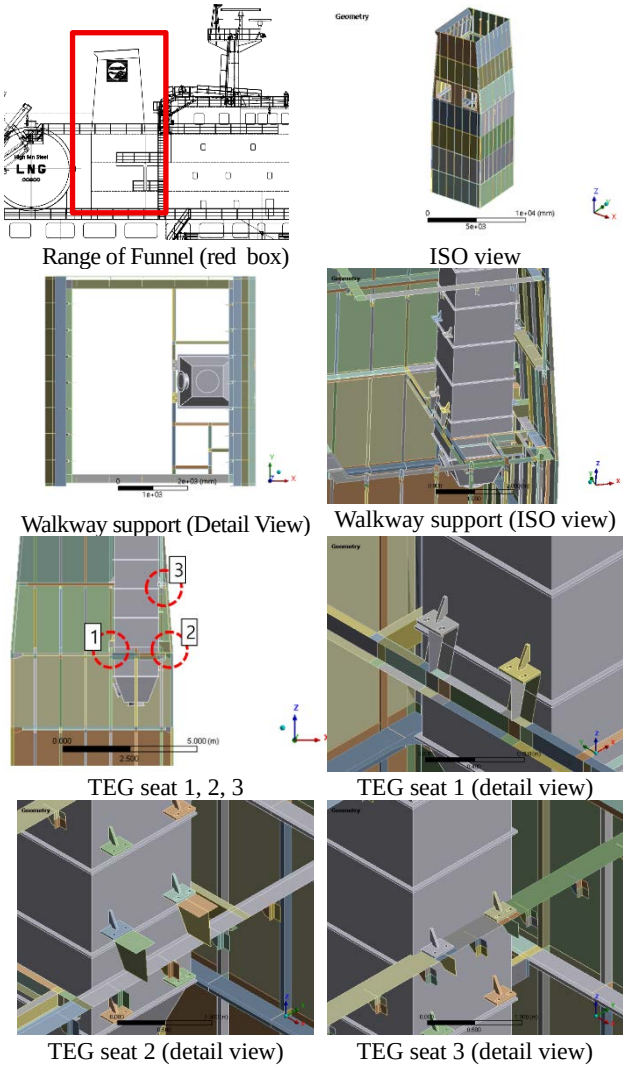

Figure 5: 3D Modeling for Structural Analysis

4.2 Finite Element Model

The funnel wall, stiffeners, walkway supports, seats, brackets and lugs were modeled with four-node, quadrilateral-dominant shell

elements (SHELL181) with their actual plate thicknesses: 7 mm for the funnel wall, 7 mm (web) and 11 mm (face plate) for the vertical stiffeners, 26 mm for the TEG seats, seat brackets and lugs, and an I-section of 200 × 90 × 8/13.5 mm for the walkway supports. The mesh was generated with the default global element size of ANSYS Mechanical, with a local body sizing of 40 mm applied to the funnel stiffeners and an edge sizing of 10 mm applied along the contact edges between the TEG lugs and the I-shaped walkway supports. The finite element model of the initial configuration consists of 544,650 nodes and 468,824 elements (**Figure 6**).

The TEG itself was not discretized. Its total wet weight of 17,250 kg was assigned as a point mass at the center of gravity, which was connected to the lug plates through joints with rigid behavior, and each lug plate was connected to the top plate of its seat by bonded contact. The TEG was idealized as a rigid body because its interior consists of a large number of complex steel members, and the purpose of the analysis was to assess the structural safety of the supports and the funnel rather than of the TEG itself. Under this assumption, the TEG imposes compatible rigid-body displacements on all supported lugs, so that the inertial loads are distributed among the lugs according to the relative stiffness of their supporting members. The flexibility of the TEG casing, which may redistribute part of the load between the lugs, is not represented; its influence on the distribution of the support loads was not quantified in this study.

All nodes at the lower cut section of the funnel were fully constrained in six degrees of freedom. The self-weight of the funnel structure was derived from the material density and plate thickness. Gravitational acceleration and the ship motion accelerations listed in **Table 3** were applied as inertial loads in the X, Y, and Z directions. The constrained section is located 9.04 m below the lowest supported lugs (No. 1 lugs on the stern side and No. 2 lugs on the bow side), so that the local stresses at the supports are not influenced by the boundary condition.

All analyses were performed using ANSYS Mechanical 2026 R1 (ANSYS Inc., USA) [**15**].



Plan view

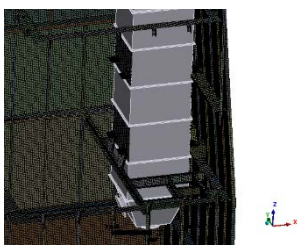

TEG support (Detail view)



TEG seat 1 (detail view) TEG seat 2 (detail view)

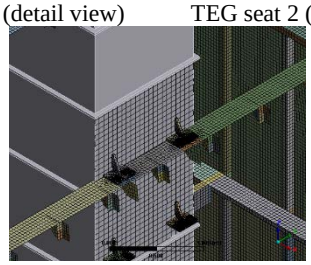

TEG seat 3 (detail view)

Figure 6: Finite Element Model for Structural Analysis

Table 3: Load Combinations Based on Loading Conditions (accelerations in units of g)

CASE No.	S	D			Remark
		A_X	A_Y	A_Z	
1	1.000	-0.293	0.000	-0.174	*D.L + S.M (HSM-1)*
2	1.000	0.293	0.000	0.174	*D.L + S.M (HSM-2)*
3	1.000	-0.355	0.000	-0.253	*D.L + S.M (HSA-1)*
4	1.000	0.355	0.000	0.253	*D.L + S.M (HSA-2)*
5	1.000	0.062	0.000	0.078	*D.L + S.M (FSM-1)*
6	1.000	-0.062	0.000	-0.078	*D.L + S.M (FSM-2)*
7	1.000	0.000	-0.900	0.163	*D.L + S.M (BSR-1P)*
8	1.000	0.000	0.900	-0.163	*D.L + S.M (BSR-2P)*
9	1.000	0.000	0.900	0.163	*D.L + S.M (BSR-1S)*
10	1.000	0.000	-0.900	-0.163	*D.L + S.M (BSR-2S)*
11	1.000	-0.094	-0.361	0.441	*D.L + S.M (BSP-1P)*
12	1.000	0.094	0.361	-0.441	*D.L + S.M (BSP-2P)*
13	1.000	-0.094	0.361	0.441	*D.L + S.M (BSP-1S)*
14	1.000	0.094	-0.361	-0.441	*D.L + S.M (BSP-2S)*
15	1.000	0.144	-0.107	0.290	*D.L + S.M (OST-1P)*
16	1.000	-0.144	0.107	-0.290	*D.L + S.M (OST-2P)*
17	1.000	0.144	0.107	0.290	*D.L + S.M (OST-1S)*
18	1.000	-0.144	-0.107	-0.290	*D.L + S.M (OST-2S)*
19	1.000	0.433	-0.139	0.412	*D.L + S.M (OSA-1P)*
20	1.000	-0.433	0.139	-0.412	*D.L + S.M (OSA-2P)*
21	1.000	0.433	0.139	0.412	*D.L + S.M (OSA-1S)*
22	1.000	-0.433	-0.139	-0.412	*D.L + S.M (OSA-2S)*

Where
D.L = Dead Load
S.M = Ship Motion

4.3 Structural Analysis

Following the design load scenario approach specified in the IACS Common Structural Rules (CSR) for Bulk Carriers and Oil Tankers **[16]**, the strength assessment was carried out for all relevant design load scenarios, and the governing condition was taken as the one producing the most unfavorable stress. Each design load scenario combines the static load with the corresponding dynamic ship-motion acceleration components. The resulting load

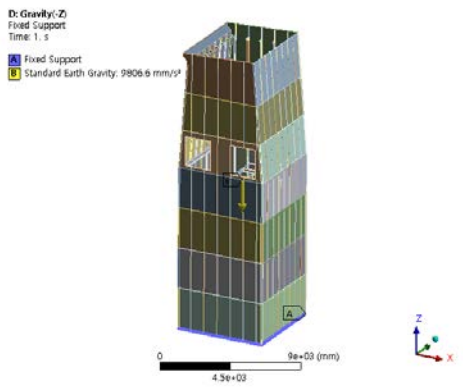

Figure 7: Static Load (S) and Boundary Condition

Table 4: Characteristics of Mass and Material Behavior in Funnel and TEG

Component	Material	Mass (kg)	Remark
TEG	SS400	17,250	RIGID BODY
Funnel Structure	SS400	34,838	FLEXIBLE BODY
Total	-	52,088	-

Table 5: Mechanical and Physical Properties of Materials

Material	E (MPa)	S_y (MPa)	S_u (MPa)
SS400	202,350	235	400

combinations are summarized in **Table 3**.

Static Load (S)

Static loads acting on the structure are illustrated in **Figure 7**. The weight of the TEG varies depending on whether it is in the dry or wet condition; since coolant is contained during operation, the wet weight of 17,250 kg was applied as the static load. The characteristics of the funnel structure and TEG were considered and were specified in **Tables 4** and **5**. The mechanical properties of SS400 were obtained from JIS G3101 **[17]**. Since SS400 is not among the ASME-designated materials listed in ASME Section II, Part D, the allowable-stress derivation methodology of ASME Section VIII, Division 2 **[18]**, as established in ASME Section II, Part D, Mandatory Appendix 10 **[19]**, was applied to the SS400 yield and tensile strength values rather than obtaining the allowable stress by direct table lookup.

Dynamic Load (D)

The dynamic loads considered in the structural analysis are the vessel acceleration effects induced by wave loads. Ship accelerations were applied in each direction (X, Y, and Z) as shown in **Figure 8** and their magnitudes are expressed as load factors in **Table 3**.

The ship-motion accelerations at the TEG were derived from the formulas of the IACS Common Structural Rules, Pt 1, Ch 4, Sec 3 **[16]**. The motions and accelerations at the center of gravity of the ship were first calculated for the full load (homogeneous loading) condition at the scantling draft, with the rule length L = 125.17 m as defined in Pt 1, Ch 1, Sec 4 of the CSR (which differs from the length between perpendiculars of 126.0 m in **Table 1**), B = 23.0 m, D = 13.5 m, $T_{LC} = T_{SC} = 9.5$ m and $C_B = 0.773$, the roll radius of gyration $k_r = 0.35B$ and metacentric height GM = 0.12B given in Pt 1, Ch 4, Sec 3, **Table 2**, $f_{BK} = 1.2$ (no bilge keel) and $f_{ps} = 1.0$ for the extreme sea load design load scenario. This gives an acceleration parameter $a_0 = 0.545$, a roll period of 11.18 s and roll angle of 34.0°, a pitch period of 9.81 s and pitch angle of 15.0°, and $a_{surge} = 1.07$ m/s^2, $a_{sway} = 1.60$ m/s^2, $a_{heave} = 5.35$ m/s^2, $a_{roll} = 0.188$ rad/s^2 and $a_{pitch} = 0.117$ rad/s^2.

Because the TEG is located far from the center of rotation of the ship, these accelerations were transferred to the center of gravity of the TEG (x = 12.75 m forward of the aft end of L, y = 0 m, z = 24.5 m above the baseline) using the formulas for accelerations at any position in Pt 1, Ch 4, Sec 3, [3.2] **[16]**:

$$a_X = -C_{XG}\, g \sin\varphi + C_{XS}\, a_{surge} + C_{XP}\, a_{pitch}\,(z - R)$$

$$a_Y = C_{YG}\, g \sin\theta + C_{YS}\, a_{sway} - C_{YR}\, a_{roll}\,(z - R)$$

$$a_Z = C_{ZH}\, a_{heave} + C_{ZR}\, a_{roll}\, y - C_{ZP}\, a_{pitch}\,(x - 0.45L)$$

where θ and φ are the roll and pitch angles, and $R = \min(D/4 + T_{LC}/2, D/2) = 6.75$ m is the vertical coordinate of the rotation center. The lever arm $z - R = 17.75$ m amplifies the rotational components; for example, in the beam sea roll cases (BSR) the roll term $a_{roll}(z - R) = 3.33$ m/s^2 is added to the gravity component $g \sin\theta = 5.49$ m/s^2, giving a transverse acceleration of 0.90g at the TEG. As required by the rules, the accelerations include the gravity components due to the instantaneous roll and pitch angles.

The load combination factors C were taken from Pt 1, Ch 4, Sec 2, **Tables 3 to 6 [16]** for the seven equivalent design waves of the strength assessment: head sea maximum vertical bending moment (HSM), head sea maximum vertical acceleration (HSA), following sea maximum vertical bending moment (FSM), beam sea maximum roll (BSR), beam sea maximum pressure (BSP), oblique sea maximum torsion (OST) and oblique sea maximum pitch acceleration (OSA). HSM, HSA and FSM are each defined for two opposite phases (-1, -2), and BSR, BSP, OST and OSA additionally for waves from port and starboard (P, S), which gives $3 \times 2 + 4 \times 4 = 22$ load cases. The rules provide envelope

accelerations as advisory values for machinery and crane foundations (Pt 1, Ch 4, Sec 3, [3.1.3]); in this study the 22 dynamic load cases were used instead so that the phase relation between the acceleration components is preserved. Because the funnel and the TEG supports are rigidly connected to the hull, they follow the rigid-body motion of the ship, and the accelerations at the TEG position obtained from these formulas apply to them directly. In each load case the static load (S, 1.0g downward) was combined with the dynamic accelerations (D) listed in **Table 3**, and the inertial loads were applied to both the TEG mass and the funnel structure.

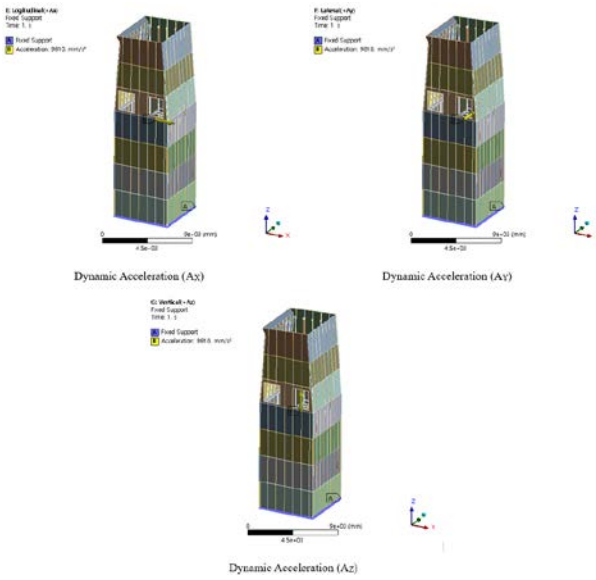

Figure 8: Dynamic Load (D) and Boundary Condition

Stress Evaluation Criteria

The stresses obtained from the finite element analysis were evaluated by the design-by-analysis method of ASME Section VIII, Division 2, Part 5 **[18]**. In this method, the stress at a section is linearized through the thickness and classified into general primary membrane stress (P_m), local primary membrane stress (P_L), primary bending stress (P_b), secondary stress (Q) and peak stress (F), and a separate allowable limit is applied to each category: $P_m \leq S$, $P_L \leq 1.5S$, $P_L + P_b \leq 1.5S$, and the range of $P_L + P_b + Q \leq S_{PS}$, where $S_{PS} = \max(3S, 2S_y)$ **[18]**. The peak stress F is the increment above the linearized stress caused by local discontinuities such as weld toes and notches; because it does not cause noticeable distortion, it is not limited in the static strength assessment but is used in the fatigue assessment **[18]**. Since the loads in this study are transmitted locally through the TEG support lugs, the stresses at the members of interest were classified as P_L, and P_L and $P_L + P_b$ were evaluated, as described in Section 4.4.

The allowable stress S of SS400 was determined following the criteria for establishing maximum allowable stress values in ASME Section II, Part D, Mandatory Appendix 10 **[19]** as $S = \min(S_y/1.5, S_u/2.4) = \min(156.7\ \text{MPa}, 166.7\ \text{MPa}) = 156.7\ \text{MPa}$, where $S_y = 235$ MPa and $S_u = 400$ MPa are the yield and tensile strengths given in **Table 5 [17]**. The limit applied to both P_L and $P_L + P_b$ is therefore $1.5S = 235$ MPa.

The ASME criteria were adopted because the ship structural rules do not provide a stress classification for local equipment supports; nevertheless, their relation to the ship structural requirements was examined. In the direct strength analysis of the IACS Common Structural Rules (Pt 1, Ch 7, Sec 2, [5.2]) **[16]**, the yield utilization factor $\lambda_y = \sigma_{vm}/R_Y$, where σ_{vm} is the von Mises membrane stress at the mid-plane of the shell element and $R_Y = 235/k$ MPa is the nominal yield stress, must not exceed $\lambda_{y\text{-}perm} = 1.0$ for the static plus dynamic (S+D) load combinations. For SS400, whose minimum yield strength (235 MPa) is equal to that of normal-strength hull steel, k = 1.0 was assumed, so that the CSR limit becomes 235 MPa and coincides with the 1.5S limit applied here to P_L. Because the CSR criterion is applied to the membrane stress only, whereas in this study the same limit is also applied to $P_L + P_b$, the present criterion is the more stringent one. For fine-mesh analyses, the CSR permits higher utilization factors, $\lambda_{fperm} = 1.5$ to 1.7 for S+D (Pt 1, Ch 7, Sec 3, [6.2.1]) **[16]**. The criterion adopted in this study is therefore equivalent to, or more conservative than, the yield criterion of the ship structural rules.

4.4 Results of Structural Analysis

Structural analyses were performed for 22 cases in accordance with the load combinations listed in **Table 3**, and **Tables 6** and **7** present, for each structural component, the maximum stresses over the 22 load cases. The results were evaluated in terms of local primary membrane stress (P_L) and membrane plus bending stress ($P_L + P_b$), following the stress classification and evaluation criteria specified in ASME Section VIII, Division 2, Part 5 **[18]**. In the shell model, P_L was taken as the von Mises equivalent stress at the mid-surface of the shell elements, which contains only the membrane components, and $P_L + P_b$ as the larger of the von Mises equivalent stresses at the top and bottom surfaces, which contain both the membrane and bending components. Because the stress in a shell element varies linearly through the thickness, these values correspond directly to the linearized membrane and membrane plus bending stresses, and no separate through-thickness linearization was

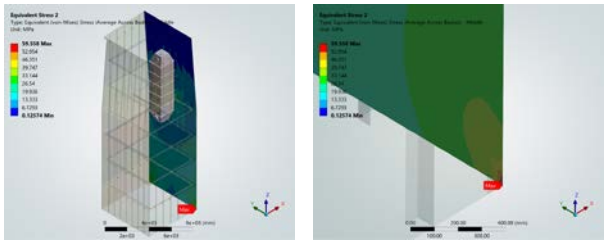

Funnel Wall: Local Membrane Stress (Max. σ = 59.55 MPa)

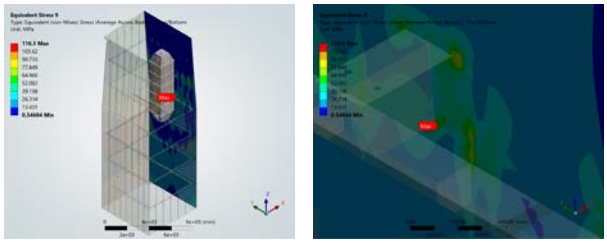

Funnel Wall: Membrane + Bending Stress (Max. σ = 116.50 MPa)

Figure 9: Equivalent Stress Distribution: Funnel Wall

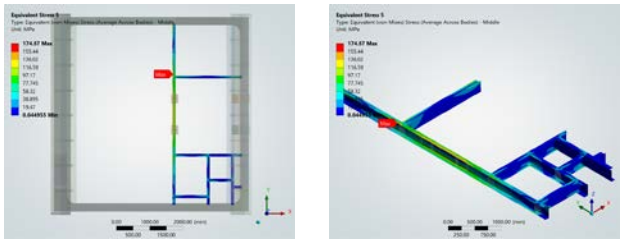

Walkway Support: Local Membrane Stress (Max. σ = 174.87 MPa)

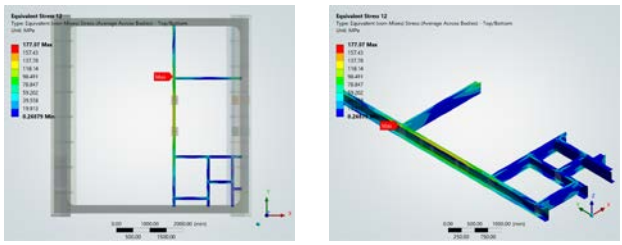

Walkway Support: Membrane + Bending Stress (Max. σ = 177.07 MPa)

Figure 10: Equivalent Stress Distribution: Walkway support

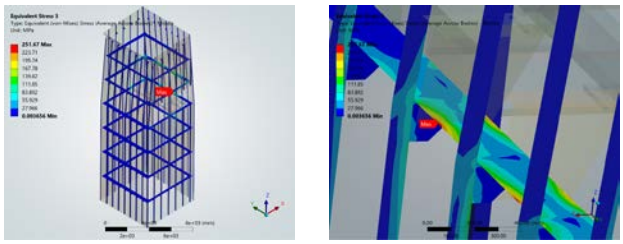

Vertical Stiffener: Local Membrane Stress (Max. σ = 251.67 MPa)

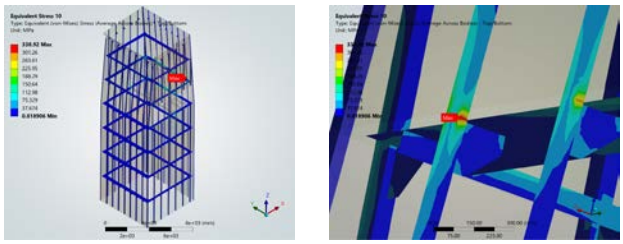

Vertical Stiffener: Membrane + Bending Stress (Max. σ = 338.92 MPa)

Figure 11: Equivalent Stress Distribution: Vertical Stiffener

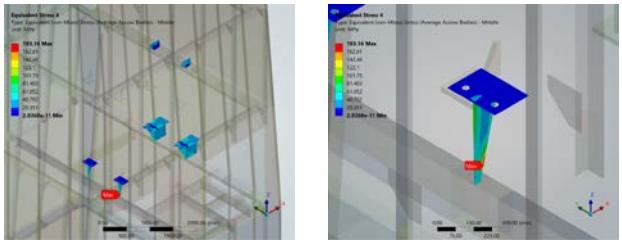

TEG Support : Local Membrane Stress (Max. σ = 183.16 MPa)

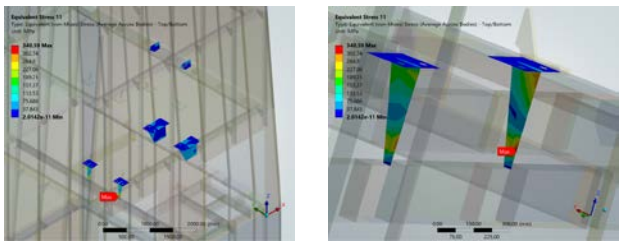

TEG Support : Membrane + Bending Stress (Max. σ = 340.59 MPa)

Figure 12: Equivalent Stress Distribution: TEG support

Table 6: Maximum Local Membrane Stress

Component	Max. Local Membrane Stress, σ (MPa)	Max. σ < 1.5S = 235 MPa
Funnel Wall	59.55	**Satisfied**
Walkway Support	174.87	**Satisfied**
Vertical Stiffener	251.67	**Not satisfied**
TEG Support	183.16	**Satisfied**

Table 7: Maximum Membrane + Bending Stress

Component	Max. Membrane + Bending Stress, σ (MPa)	Max. σ < 1.5S = 235 MPa
Funnel Wall	116.50	**Satisfied**
Walkway Support	177.07	**Satisfied**
Vertical Stiffener	338.92	**Not satisfied**
TEG Support	340.59	**Not satisfied**

required. The von Mises stress was calculated from all in-plane normal and shear stress components at each surface, and the nodal stresses were averaged, including across the boundaries of connected bodies (Average Across Bodies option of ANSYS Mechanical), which reduces the influence of single-element peaks at the junctions of the members. The TEG loads are introduced into the funnel structure only at the lugs, seats and walkway supports, which are structural discontinuities. As shown in **Figures 9 to 12**, the maximum membrane stresses of the principal members occur in the vicinity of these load-introduction points and decrease away from them; they were therefore classified as P_L and assessed against 1.5S. P_m, which applies to general regions remote from discontinuities, was not evaluated separately: for the funnel wall, even the maximum membrane stress including the regions adjacent to the seats (59.55 MPa) is well below S = 156.7 MPa, so that the P_m criterion is satisfied, whereas the vertical stiffeners, walkway supports and seats are short load-

transfer members whose membrane stresses are governed by the local load introduction from the lugs.

The funnel wall satisfied the allowable limit for both P_L and $P_L + P_b$, and the walkway support was also within the limit (174.87 and 177.07 MPa, respectively). The vertical stiffener exceeded the limit for both P_L (251.67 MPa) and $P_L + P_b$ (338.92 MPa), and the TEG support exceeded it for $P_L + P_b$ (340.59 MPa), whereas its P_L (183.16 MPa) was within the limit. Additional reinforcement schemes are therefore proposed in order to examine the feasibility of relieving these local stresses.

4.5 Structural Strengthening for Reduction of Localized Stress Concentration

To relieve local stress concentrations, all lugs of the TEG were utilized. Similar to how the existing walkway supported the first set of lugs on the stern side, an additional walkway was designed to support the second set of lugs. Brackets were installed on all four sets of lugs on the bow side, and to enhance structural support, the single-bracket design was modified into a pair of brackets. This modification was equally applied to the stern side, as illustrated in **Figure 13**. The finite element model of the reinforced configuration was generated from the same geometry and with the same meshing conditions as the initial model described in Section 4.2, differing only in the added reinforcement members, and consists of 550,235 nodes and 474,797 elements. The stresses of the two configurations can therefore be compared directly.

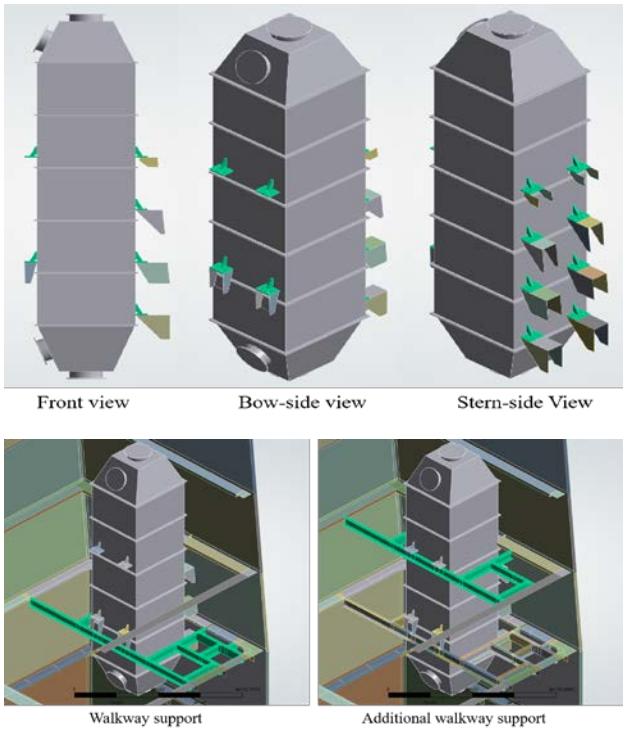

Figure 13: Information on Structural Reinforcements for Structural Analysis

4.6 Results of Structural Strengthening Analysis

The structural analysis was repeated under the same load conditions after the reinforcement. As shown in **Figures 14** to **17**, the stresses acting on the funnel wall, walkway support, vertical stiffener, and TEG support were distributed more uniformly than in the original configuration. The maximum stresses of the principal components are listed in **Tables 8** and **9**, which confirm that even the concentrated local stresses fall within the allowable limits. As in the initial configuration, the maximum membrane stresses occur in the vicinity of the load-introduction points (**Figures 14** to **17**), and the maximum membrane stress of the funnel wall (52.77 MPa) remains below S = 156.7 MPa; the stress classification described in Section 4.4 therefore applies to the reinforced configuration as well. For the reinforced configuration, the governing load case was OSA-1P (case 19) for the walkway support and TEG support for both P_L and $P_L + P_b$, and for the vertical stiffener OSA-1S (case 21) for P_L and OSA-1P (case 19) for $P_L + P_b$; for the funnel wall, P_L was governed by BSR-1S (case 9) and $P_L + P_b$ by OSA-1S (case 21). The oblique sea cases combine the largest longitudinal acceleration (0.433g) with a large vertical acceleration (0.412g), which, because of the height of the TEG, produce large overturning moments at the support lugs.

These results will be provided as reference material during the selection of the retrofit shipyard and utilized in adjusting the ex-

Table 8: Maximum Local Membrane Stress after Strengthening

Component	Max. Local Membrane Stress, σ (MPa)	Max. σ < 1.5S = 235 MPa
Funnel Wall	52.77	**Satisfied**
Walkway Support	157.22	**Satisfied**
Vertical Stiffener	163.20	**Satisfied**
TEG Support	140.31	**Satisfied**

Table 9: Maximum Membrane + Bending Stress after Strengthening

Component	Max. Membrane + Bending Stress, σ (MPa)	Max. σ < 1.5S = 235 MPa
Funnel Wall	127.14	**Satisfied**
Walkway Support	180.51	**Satisfied**
Vertical Stiffener	222.72	**Satisfied**
TEG Support	149.82	**Satisfied**

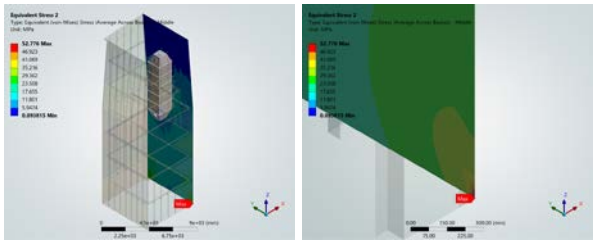

Funnel Wall: Local Membrane Stress (Max. σ = 52.77 MPa)

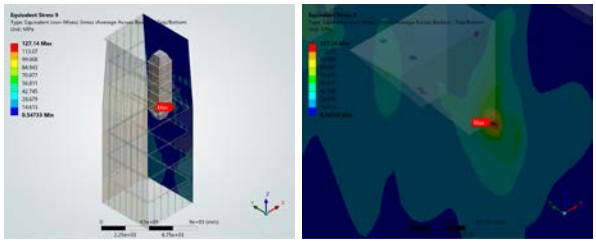

Funnel Wall: Membrane + Bending Stress (Max. σ = 127.14 MPa)

Figure 14: Equivalent Stress Distribution: Funnel Wall

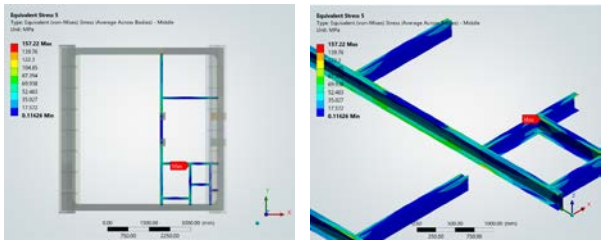

Walkway Support: Local Membrane Stress (Max. σ = 157.22 MPa)

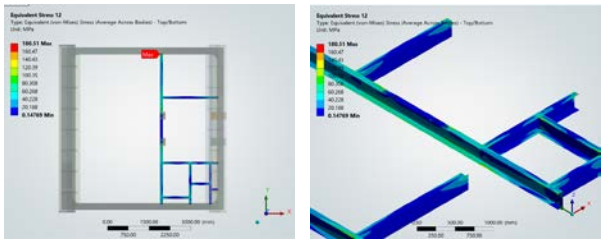

Walkway Support: Membrane + Bending Stress (Max. σ = 180.51 MPa)

Figure 15: Equivalent Stress Distribution: Walkway support

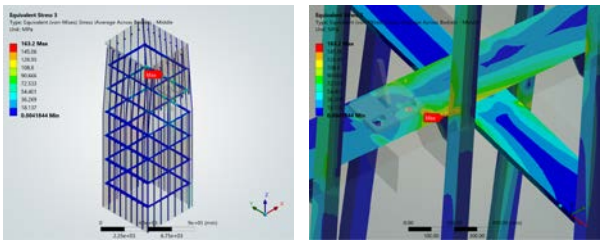

Vertical Stiffener: Local Membrane Stress (Max. σ = 163.20 MPa)

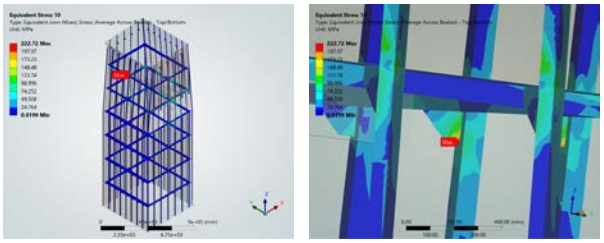

Vertical Stiffener: Membrane + Bending Stress (Max. σ = 222.72 MPa)

Figure 16: Equivalent Stress Distribution: Vertical Stiffener

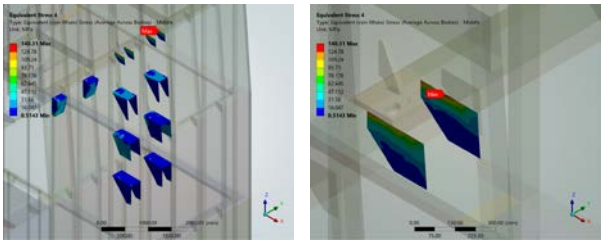

TEG Support : Local Membrane Stress (Max. σ = 140.31 MPa)

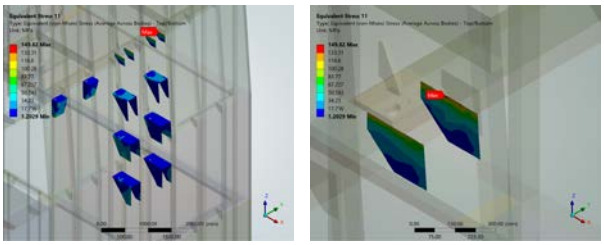

TEG Support : Membrane + Bending Stress (Max. σ = 149.82 MPa)

Figure 17: Equivalent Stress Distribution: TEG support

tent of reinforcement. Following the installation, a 1,000-hour operational demonstration onboard the vessel is planned to validate the performance of the developed TEG system under actual sea conditions.

4.7 Limitations of the Present Assessment

The present assessment is a quasi-static strength evaluation in which the ship-motion accelerations are applied as equivalent inertial loads. The following effects, which are relevant to the planned onboard operation, are not covered by the analysis and are therefore discussed here as limitations.

First, vibration. The TEG and its supports are exposed to excitation from the main engine and propeller, transmitted through the deckhouse, and from the exhaust gas flow. For the six-cylinder main engine of KOMERI1 (124 rpm at SMCR), the first-order and firing (sixth-order) excitation frequencies are approximately 2.1 Hz and 12.4 Hz, respectively. Because the TEG was represented as a rigid body connected through rigid joints, the natural frequencies of the TEG–support system were not evaluated, and resonance with these excitation sources cannot be excluded by the present analysis. A modal analysis of the reinforced configuration including the mass and stiffness of the TEG is required before installation.

Second, thermal expansion. The TEG casing is heated by the exhaust gas, whereas the funnel structure remains close to ambient temperature. If the differential thermal expansion between the casing and its supports, or between the TEG and the connected exhaust ducts, is restrained, secondary stresses (Q) arise at the lugs and seats. These stresses were not included in the present analysis; the support arrangement should accommodate thermal

movement, for example by means of sliding supports and expansion joints in the exhaust ducts, and the resulting $P_L + P_b + Q$ range should be checked against the S_{PS} limit.

Third, fatigue. Wave-induced loads act on the supports for a very large number of cycles over the service life of the ship (of the order of 10^7 to 10^8), and engine-induced vibration adds high-frequency cycles. The support connections identified as the most highly stressed members in this study are the locations where fatigue cracks are most likely to initiate; however, a fatigue assessment based on the long-term distribution of wave loads, such as that specified in the ship structural rules, was beyond the scope of this study. In addition, the local stresses at the weld connections of the supports depend on the mesh size, and a systematic mesh-sensitivity study was not performed; the narrow margin of the vertical stiffener (5.2%) should therefore be considered in the final reinforcement design.

Fourth, buckling. The 7 mm funnel wall and the slender vertical stiffeners are subjected to compressive stresses from the overturning moment of the eccentric TEG mass of 17,250 kg, which is largest in the oblique sea cases. Local plate and stiffener buckling was not evaluated in the present linear static analysis and should be checked, for example by the buckling criteria of the ship structural rules or by a linear eigenvalue buckling analysis, when the reinforcement design is finalized. Accordingly, the conclusions of this study are limited to the static strength of the support structure under the design ship-motion accelerations.

5. Conclusion

Two rounds of finite element analysis were performed to evaluate the structural integrity of the support structure inside the funnel for the installation of the TEG under 22 load combinations derived from the ship-motion accelerations of the IACS Common Structural Rules. The main conclusions are as follows.

(1) In the initial configuration, the funnel wall and walkway support satisfied the allowable limit, whereas the vertical stiffener exceeded the 1.5S limit of 235 MPa for both P_L (251.67 MPa) and $P_L + P_b$ (338.92 MPa), and the TEG support exceeded it for $P_L + P_b$; the largest membrane plus bending stress, 340.59 MPa, occurred in the TEG support.

(2) Utilizing all lugs of the TEG, i.e., supporting the No. 1 and No. 3 lugs on the bow side with additional seats and the No. 2 lugs on the stern side with an additional walkway support, and replacing the single brackets with pairs of brackets, redistributed the loads. The maximum membrane plus bending stresses of the vertical stiffener and TEG support were reduced from 338.92 and 340.59 MPa to 222.72 and 149.82 MPa, respectively. The stresses in the funnel wall and walkway support increased slightly, from 116.50 to 127.14 MPa and from 177.07 to 180.51 MPa, because part of the TEG load is transferred through the additional seats and walkway support, but they remained within the limit, and all principal members satisfied the allowable limits.

(3) The vertical stiffener retains a margin of only about 5.2% under the membrane plus bending criterion (222.72 MPa against 235 MPa), which should be considered when the reinforcement design is finalized and during subsequent inspection.

(4) These conclusions are limited to the quasi-static strength of the support structure. Vibration, thermal expansion, fatigue and buckling, discussed in Section 4.7, are to be assessed before and during the planned 1,000-hour operational demonstration onboard the vessel, together with structural monitoring of the reinforced members.

Acknowledgement

This work was supported by Korea Institute of Energy Technology Evaluation and Planning (KETEP) grant funded by the Korea government (MOTIE) (RS-2021-KP002414).

Author Contributions

Conceptualization, S. H. Jeong and Y. S. Yun; Methodology, S. H. Jeong; Software, S. H. Jeong; Validation, S. H. Jeong and S. Y. Choi; Formal Analysis, S. H. Jeong; Resources, S. H. Jeong and S. Y. Choi; Data Curation, S. H. Jeong; Writing—Original Draft Preparation, S. H. Jeong and M. H. Lee; Writing—Review & Editing, M. H. Lee and Y. S. Yun; Visualization, S. H. Jeong; Supervision, Y. S. Yun; Project Administration, S. Y. Choi; Funding Acquisition, S. H. Jeong and S. Y. Choi.

References

[1] IMO. Rules on ship carbon intensity and rating system enter into force. IMO Media Centre Press Briefings, 1 November 2022.

[2] IMO. 2023 IMO Strategy on Reduction of GHG Emissions from Ships. International Maritime Organization.

[3] S. D. Kim, S. J. Yun, and J. H. Kim, Study on physical modeling and simulation of a maritime substantiation vessel for verifying the operational efficiency of a rotor sail. Journal of Advanced Marine Engineering and Technology, Vol.48, No.6, 480–486, 2024.

[4] J. H. Kim. A study on the effects of crescent-shaped wing sails on ship propulsion performance. Journal of Advanced Marine Engineering and Technology, Vol.49, No.4, 262–268, 2025.

[5] Korean Register (KR). IMO GHG Reduction Measures - Frequently Asked Questions, 2025.

[6] B. I. Kim, K. T. Kim, and Islam, M. S. Development of strength evaluation methodology for independent IMO Type C tank with LH2 carriers. Journal of Ocean Engineering and Technology, Vol.38, No.3, 87–102, 2024.

[7] T. Muttaqie, D. H. Jung, S. R. Cho, and J. M. Sohn, Direct strength evaluation of the structural strength of a 500 cbm LNG bunkering ship. Structural Engineering and Mechanics, Vol.81, No.6, 781–790, 2022.

[8] S. J. Cha, H. J. Tak, B. K. Hwang, J. P. Lee, J. H. Kim, and J. M. Lee, Structural assessment of independent Type-C liquid hydrogen fuel tank. Journal of Marine Science and Engineering, Vol.13, No.4, 730, 2025.

[9] W. Nam, S. J. Park, and K. Kim, Numerical investigation of the ultimate strength of D-ring devices and deck structures. Journal of Marine Science and Engineering, Vol.10, No.7, 952, 2022.

[10] D. M. Kim, S. H. Hong, S. H. Jeong, Analysis of dynamic characteristics of rotor sail using a 4DOF rotor model and finite element model. Journal of Marine Science and Engineering, Vol.12, No.2, 335, 2024.

[11] L. Ao, Z. Ding, B. Liu, Z. Pei, Q. Tang, and W. Wu, Experimental and numerical analysis of ultimate carrying capacity of a funnel structure with opening under wind pressure. Journal of Marine Science and Engineering, Vol.12, No.1, 41, 2024.

[12] H. W. Jeong, Development of a funnel-integrated SOx scrubber. Bulletin of the Society of Naval Architects of Korea, Vol.56, No.1, 34–38, 2019 (in Korean).

[13] General Arrangement of D/W 17,000 ton-class Bulk Carrier, Yuil co., Ltd., Accessed April 14, 2026.

[14] Specification of D/W 17,000 ton-class Bulk Carrier, Yuil co., Ltd., Accessed April 14, 2026.

[15] ANSYS Inc., ANSYS Mechanical, Release 2026 R1, Canonsburg, PA, USA: ANSYS Inc., 2026.

[16] International Association of Classification Societies, Common Structural Rules for Bulk Carriers and Oil Tankers (CSR-BC & CSR-OT), London, UK: IACS, 2025.

[17] Japanese Industrial Standards Committee, JIS G 3101: Rolled Steels for General Structure, Tokyo, Japan: JISC, 2016.

[18] ASME, Boiler and Pressure Vessel Code, Section VIII, Division 2: Rules for Construction of Pressure Vessels - Alternative Rules, Part 5: Design by Analysis, New York, NY, USA: The American Society of Mechanical Engineers, 2023.

[19] ASME, Boiler and Pressure Vessel Code, Section II, Part D: Properties (Metric), Mandatory Appendix 10 — Basis for Establishing Maximum Allowable Stress Values for Tables 5A and 5B, New York, NY, USA: The American Society of Mechanical Engineers, 2015.